Investigating the Character of Excited States in TiO_2 Nanoparticles from Topological Descriptors: Implications for Photocatalysis†

Rosendo Valero,* Ángel Morales-García and Francesc Illas

Departament de Ciència de Materials i Química Física & Institut de Química Teòrica i Computacional (IQTCUB), Universitat de Barcelona. c/ Martí i Franquès 1-11, 08028 Barcelona, Spain

*E-mail: rosendo.valero@ub.edu

Abstract

Titanium dioxide (TiO_2) nanoclusters (NCs) and nanoparticles (NPs) have been the focus of intense research in recent years since they play a prominent role in photocatalysis. In particular, the properties of their excited states determine the photocatalytic activity. Among the requirements for photocatalytic activity, low excitation energy and large separation of the charge carriers are crucial. While information regarding the first is straightforward either from experiment or theory, the information regarding the second is scarce or missing. In the present work we fill this gap through a topological analysis of the first singlet excited state of a series of TiO_2 NCs, anatase and rutile derived NPs containing up to 495 atoms. The excited states of all these systems in vacuo has been obtained from time-dependent density functional theory (TDDFT) calculations using hybrid functionals and the influence of water taken into account through a continuum model. Three different topological descriptors are scrutinized that are derived from the attachment/detachment one-electron charge density. These are to (*i*) charge transfer degree, (*ii*) charge density overlap, and (*iii*) distance between centroids of charge. The present analysis shows that the charge separation in the excited state strongly depends on the NP size and shape. The character of the electronic excitations, as arising from the analysis of the canonical Kohn-Sham molecular orbitals (MOs) or from natural transition orbitals (NTOs) is also investigated. The understanding and prediction of charge transfer and recombination in TiO_2 nanostructures may have implications in the rational design of these systems to boost their photocatalytic potential.

† Electronic supplementary information (ESI) available: Detailed equations that define the topological descriptors. TDDFT PBE0 topological descriptors for nanoclusters (Table S1), TDDFT optical gap for nanoclusters (Table S2), optical gaps, excited state character, and weight of NTOs for nanoparticles at TDDFT PBE0 level (Table S3), TDDFT NTOs for nanoclusters with PBEx functional (Fig. S1) and with PBE0 functional (Fig. S2), TDDFT NTOs for nanoparticles (Fig. S3), centroids for nanoclusters at TDDFT PBEx level (Fig. S4), and centroids for nanoparticles at TDDFT level (Fig. S5).

1. Introduction

Since Fujishima and Honda first reported the overall photocatalytic water splitting by using a Titanium dioxide (TiO_2) electrode in 1972,[1] TiO_2 nanostructures have been the object of a large number of studies aimed to better understand the intricacies of photocatalysis.[2-6] In fact, the photocatalytic activity of TiO_2 results from many factors involving, morphology, size and nature of charge carriers. Interestingly, the latter one is directly associated to the formation of the photogenerated hole (h^+) and electron (e^-) species under irradiation and plays a key role in the photocatalytic process. The efficiency of a photocatalyst can be measured by the redox reactions performed by such photogenerated carriers over adsorbed species on the photocatalyst surface, or by their recombination.[7] Not surprisingly, the efficiency of a given photocatalyst could be highly improved by suppressing the carrier recombination step and consequently prolonging the lifetime of the e^-–h^+ pair, which is also called exciton.[8] Charge separation in TiO_2, rather than charge transfer to reactants or intermediates, seems to be the rate controlling step in photocatalytic processes.[9] In fact, one of the reasons why the TiO_2 anatase phase exhibits higher photocatalytic activity than the rutile TiO_2 one is attributable to their larger carrier lifetimes.[10] However, the carrier lifetime is not the only factor responsible for the photocatalytic activity, as mentioned earlier. Recent studies have suggested that the size and the shape of TiO_2 nanostructures directly influence their performance in the photocatalytic applications and hence they have a notable effect on the generation, recombination, separation and diffusion rates of the exciton.[11-19]

The valuable information that one can obtain from the localization and identification of the exciton quasiparticle in molecules, nanoclusters (NCs) and nanoparticles (NPs) has motivated the development of several theoretical approaches aimed at qualitatively and quantitatively describing the properties of the relevant excited states and to provide appropriate chemical descriptors. These descriptors, based on excited state quantum chemistry methods, such as time-dependent density functional theory (TDDFT), allow one to characterize the topology of the electronic transition, particularly in what concerns its character as a local valence or charge-transfer excitation. Excited states with long-range charge transfer are known to be problematic to TDDFT,[20] and motivated the introduction of descriptors such as the Λ index proposed by Tozer *et al.*[21,22] Essentially, this index is a weighted and normalized sum over all excitations of the spatial overlap between the occupied and virtual orbitals participating in the excitation; a low Λ corresponds to a long-range charge transfer excitation. Later, a number of measures of charge transfer based on the spatial extent of the transition, derived either from the difference density between the excited and the ground state or from the distance between orbital centroids, were proposed.[23-27] Recently, Etienne *et al.*[28-31] introduced a strategy to retrieve crucial topological information related to charge transfer from the so-called detachment/attachment density matrices[32] and natural transition orbitals (NTOs),[33,34] and suggested to use the detachment/attachment densities, which also physically depict the electron/hole generated by electronic transition. Mewes *et al.*[35] carried out a benchmarking on a series of excited states of different systems by exploiting the concept of excitons and showing that the distance between the electron and hole centroids can be interpreted as the average distance between the hole and the electron. The same authors also proposed a complementary measure

of the exciton size that is quantified by the root-mean-square electron-hole separation, a measure that includes charge-resonance (or dynamic charge transfer).[36,37] Another density based descriptor defined as density overlap region indicator (DORI) has been developed to visualize and to quantify the electronic and geometric changes that molecular systems experience upon electronic excitations.[38] A visualization tool in the form of electron-hole maps, derived from the construction of transition density matrices, has also been proposed.[39,40] Another recent density matrix based formalism has been developed where state density matrices give rise to density plots, population analyses, and natural orbitals.[41,42] In this formalism, the transition density matrices are decomposed into NTOs (single-state and state-average) and used to define hole and electron densities. Several applications have been reported where electron-hole correlations and exciton size, and charge resonance effects were investigated, and difference density matrices used to define attachment/detachment densities.[43-46] In summary, these methods have opened a route for a rather automatic assignment of excited state features based on the electronic density and/or orbital properties only, thus leading to a deep knowledge that ultimately could lead to a rational improvement of photocatalytic materials.

To find out how the photogenerated e^- and h^+ entities participate in photocatalytic reactions on TiO_2, including water splitting for hydrogen production under sunlight, constitute a real challenge. Several computational studies have investigated the active sites at the TiO_2 surface and the TiO_2/water interface.[47-51] Additionally, a set of studies has been performed by using TDDFT with different exchange-correlation potentials to investigate the electronic structure of small $(TiO_2)_n$ NCs with n ranging from 2 to 10.[52,53] These studies tackled some features of the excitation from the point of view of the ground and excited states, with less details about exciton properties such as physical nature and/or localization. However, the later properties are important because of their direct relation to the rates of generation and recombination of charge carriers. As described earlier, it has been experimentally found that both size and shape affect the photocatalytic activity of TiO_2 NPs.[11] In this regard, nonadiabatic molecular dynamics (NAMD) simulations combined with real-time TDDFT have been employed to investigate the effect of size and shape on charge recombination in a series of TiO_2 NPs.[15] Here, the analysis of the electronic structure, nuclear dynamics, charge density, and electron-phonon coupling proved to decrease recombination rates with increased isolated NP size. A very recent report using the same methodology has shown that in reduced TiO_2 NPs there is a strong influence of the location of oxygen vacancies on the nonradiative e^-–h^+ charge trapping and recombination level.[16] Clearly, descriptors providing this type of information without requiring to rely on computationally costly and non-trivial NAMD simulations would be invaluable to classify sets of TiO_2 NPs in terms of their potential photocatalytic performance. In the present work, we show how topological-chemical descriptors based on detachment/attachment densities and NTOs can be used to gather important information of the excited state properties of stoichiometric and reduced TiO_2 NCs and NPs both in vacuo and in water. The results reported hereinafter allow us to distinguish and to classify TiO_2 NCs and NPs with different size and morphology in terms of their potential activity in photocatalysis and, hence, to provide a further step towards the rational design of TiO_2 photocatalytic nanoparticles with tailored excited state properties.

2. Computational scheme

2.1 Models of TiO_2 NCs and NPs

In the present work, we perform an analysis of the excited states of a series of $(TiO_2)_n$ (n = 1–20) NCs,[54] with structures obtained by a global optimization algorithm.[52,53,55] Furthermore, to obtain information about excited state properties of realistic NPs, we have also studied stoichiometric $(TiO_2)_n$ NPs with structures derived from the anatase bulk phase, both bipyramidal with n = 35, 84, and 165, and truncated octahedral with n = 78 and 97 NPs, and one NP derived from rutile bulk phase with n = 51. Bipyramidal TiO_2 NPs exhibit six (101) facets, whereas truncated octahedral NPs expose simultaneously (101) and (001) facets.[19] Further, the rutile NP exhibits (110), (101), and (001) facets. Besides, we have studied one reduced NP with n = 84 with an oxygen vacancy located inside the NP. Following previous work, the reduced $(TiO_2)_{84}$ NP is labelled as 84_I-3-2.[56] The starting geometry of the NPs was obtained from a Wulff construction[57] and then optimized using the PBE density functional without symmetry constraints.

2.2 Methods

The calculations for the NCs and NPs in vacuo and in water have been carried out using the hybrid PBEx[58] and PBE0[59,60] density functionals with 12.5% and 25% of Fock exchange, respectively. The standard 6-31G(d) basis sets has been used for titanium and oxygen atoms. In addition to the singlet ground state of NCs and NPs, several singlet excited states have been calculated in the framework of the vertical excitation approximation by using TDDFT. We recall that TDDFT is prone to yield spuriously low long-range charge transfer states, especially when local density approximation (LDA) or generalized gradient approximation (GGA) density functionals are employed.[61,62] The problem is ameliorated when a fraction of exact exchange is introduced, either as in global hybrids or as in range-separated functionals. This is one of the reasons we introduce here two different global hybrid functionals to try to gauge the influence of the Fock exchange on the energy and character of the excited states investigated. To further explore this issue, we have chosen the CAM-B3LYP long-range corrected density functional[63] for selected nanoparticles. We recall that CAM-B3LYP contains 19% of Fock exchange at short range and 65% of Fock exchange at long range, with the intermediate region being described by the standard error function.

For solvation, the self-consistent reaction field (SCRF) model, in which the solute is placed in a cavity within the solvent reaction field, was applied using the integral equation formalism (IEF) in the polarizable continuum model (PCM).[64] The IEFPCM method was applied both to the PBEx and PBE0 ground state and to the excited states. For the latter, the default implementation of the linear response formalism[65,66] in its non-equilibrium variant was employed. The non-equilibrium approach assumes that only the electronic component of the solvent dielectric can respond to the very fast transition from the ground to the excited states. Therefore, the optical dielectric constant instead of the static dielectric constant was used in this case. For the calculations in water, the static dielectric constant ε = 78.3553 and the optical dielectric constant ε_∞ = 1.7778 were employed in the ground state and TDDFT calculations, respectively.

The Gaussian'09[67] electronic structure package was used for the DFT and TDDFT calculations, and the NANCY_EX-2.0 [68] software was applied in the quantum chemical-topological analysis. The NANCY_EX-2.0 program carries out the post-processing of Gaussian output files and allows one to obtain topological descriptors of the excited states of a finite system such as molecules, clusters, or nanoparticles. We report results for the first singlet excited state, but we compute at least the first two singlet excited states, since in some cases the program requires that several excited states are computed. Due to Kasha's rule,[69] the first singlet excited state is expected to be the one most relevant to photocatalysis (e.g., in water splitting) in TiO_2. This is because, even if the photoexcitation accesses higher excited states, the latter are expected to experience a fast nonradiative relaxation down to the first excited state.

In the framework of the present work, it is important to remark that we focus on a TDDFT description of the excited state in the adiabatic approximation; *i.e.* the TDDFT coupling matrix is frequency independent, and in the linear response formalism. This type of TDDFT excited state has an analogous structure to a configuration interaction wave function including single excitations only (CIS).[70] Hence, the excited state can be represented by a weighted linear combination of singly-excited Slater determinants derived from a single-reference Kohn-Sham ground-state determinant, expressed in the canonical molecular orbital (MO) basis. Thus, an exciton wave function can be associated to a TDDFT excited state. One can then analyze, e.g., the first excited singlet state and determine, in principle, the e^-–h^+ contributions in the occupied/virtual canonical subspaces. Although in this way knowledge of the charge transfer features in a molecule or cluster can be gained, the fact that in general there are several coefficients in the exciton wave function expansion in a canonical MO basis makes it difficult to have a clear physical picture of the light-induced charge transfer process.

Several methods have been devised to perform a topological analysis of the excited states, as detailed previously. In the present study, we follow the formalism of Etienne *et al.*[28-31] Even though the whole formalism has been presented in the latter works, for completeness, a description including the main equations is detailed in ESI. Thus, only the topological descriptors and their meaning is presented in the following. The Φ_S descriptor is a measure of the overlap between the hole and the electron charge densities. The range of Φ_S runs from 0 to 1, the two limits corresponding to a full charge transfer transition and a completely local valence transition with full overlap between the electron and the hole, respectively. The normalized displaced charge labeled as Φ varies between zero, for a local valence transition, and one, for the full charge transfer excitation, i.e., for completely separated hole and electron densities. The intercentroid distance, i.e., the distance between the centroids of charge of the hole and the electron, can also be regarded as a topological descriptor and can also be related with Φ_S and Φ, as we will see later. Finally, natural transition orbitals (NTOs) are a type of orbitals which derive from the transition density matrix and provide a concise representation of the electronic excitations. As we will see, for many of the NCs and NPs studied here, and more in general, there is just one dominant pair of NTOs. This contrasts with the expression of the exciton wave function in canonical MOs,

where two or more pairs of singly excited transitions are often present. Thus, in the NTO basis the exciton is represented in a very compact form which is ideal for interpretative purposes.

3. Results and discussion

For a better understanding, results are reported in two separate subsections. We start discussing the topological descriptors based on the degree of charge transfer (Φ), the charge transfer overlap (Φ_S) and the distance between centroids of charge (d_c). Then, we continue with the description of the NTOs. All descriptors are discussed simultaneously for the $(TiO_2)_n$ (n =1-20) NCs, anatase (n = 35, 78, 84, 97, 165), reduced anatase 84_I-3-2 NP and rutile $(TiO_2)_{51}$ NPs.

3.1 Topological descriptors

We start by analyzing the values of the Φ, Φ_S, and d_c topological descriptors for the abovementioned TiO_2 NCs and NPs. The PBEx calculated values of these descriptors for all NCs and NPs, in vacuo and in water, are presented in Table 1 whereas PBE0 values are reported in Table S1 of the Electronic Supplementary Information (ESI). For the Φ descriptor, the calculated values are always larger than 0.85, pointing towards a clear intracluster transfer of a large fraction of an electron. In particular, it is remarkable that the value of Φ is always equal or larger for particles in gas phase than in water. This tendency is represented in Fig. 1, that shows the difference between these two sets of values for all the particles. Even though the difference is not large in relative terms, it points to an interesting behavior, namely, when the NPs feel the electrostatic effect of water as a solvent, the charge separation is less efficient. A complementary and perhaps further clear view of the nature of the electronic excitation as well as of the effect of solvation is provided by the Φ_S descriptor. The data collected in Table 1 show that, except for the n = 2 NC and the n = 84_I-3-2 NP, Φ_S is equal or larger in water than in gas phase; a trend that is clearly shown in Fig. 2. Interestingly, the magnitude of Φ_S corresponds to a relatively low overlap between the electron and the hole which, in turn, indicates a significant charge separation. Finally, according to the values listed in Table 1, the d_c value mostly decreases significantly in water as compared to values for the gas phase NPs. Furthermore, whereas in gas phase it could be stated that the first excited state is of long-range charge transfer character, in water the excitation would rather correspond to a short-range charge transfer or local valence excitation. Note that d_c for n = 2 and for n = 8 is zero. This is because these two NCs are centrosymmetric, and both electron and hole coincide with the inversion center of the cluster. This points to an already reported difficulty of the d_c descriptor for symmetric cases.[27] Nevertheless, the other descriptors characterize the excited state of the NCs in a consistent way. In order to relate the three descriptors, Fig. 3 shows the correlation between d_c and Φ_S, and between d_c and Φ. From the upper panel, it becomes clear that a low Φ_S (a low electron/hole overlap and, hence, a large charge carrier separation) also indicated a large d_c; obviously large Φ_S correspond to low d_c. Note how the solvated NCs are mostly gathered in a narrow region of large Φ_S and small d_c suggesting that such small NCs are not good candidates for photocatalysis. In the lower panel, a complementary view is obtained since a low Φ (a

low intracluster electron transfer) corresponds to a low d_c, and a large Φ corresponds to large d_c. Now the solvated NCs are confined in a reduced area of low Φ and also small d_c.

Next, the PBEx results just presented can be compared with PBE0 results in Table S1 of ESI. Focusing first on the Φ descriptor, one can observe that PBEx predicts a larger degree of charge separation than PBE0. Also, the effect of solvation on charge separation is lower for PBE0 than for PBEx. The Φ_S descriptor evidences a significantly larger electron/hole overlap for PBE0, and again a smaller effect of water solvation. As for the intercentroid distance d_c, it is also smaller for PBE0, in consistency with the values of Φ and Φ_S, but the effect of solvation on d_c is relatively large, with values in solvent being around and below 1.0 Å. In general, it seems that PBE0, with a larger contribution of Fock exchange produces a picture where electron and hole are closer together and show larger overlap and smaller charge transfer. Note that, in general, a larger amount of Fock exchange usually decreases the delocalization of the MOs. This is well-known for magnetic systems with localized spins,[71] a larger amount of Fock exchange decreases the overlap between the magnetic orbitals. For the nanoclusters the MOs change not only their shape but also their location, producing instead a larger overlap and a smaller charge transfer degree. In any case, for both PBEx and PBE0, the larger overlap between electron and hole in solvated clusters, along with the smaller charge transfer character and the smaller d_c, could indicate an increased difficulty of charge separation in condensed phase, and a concomitantly lower photocatalytic activity. Hence, even if the PBEx and PBE0 calculated descriptors differ quantitatively, they provide a consistent picture concerning the character of the excited states and the effect of water solvation. Note also that the solvation effect is much more evident for the NCs, which do not necessarily represent the situation in larger NPs of experimental relevance. Also, as an implicit solvation model for water has been applied here, we have not accounted for specific solvation effects such as hydrogen bonds, and neither have we considered the possible hydroxylation of the NP surface.

3.2. Optical gaps and natural transition orbital based analysis

The optical gap corresponds to the excitation energy to the first excited singlet and here it is estimated through TDDFT. The PBEx calculated values along with the excited state character in both canonical Kohn-Sham MO and NTO basis, are shown in Table 2 for the NPs with the corresponding results for the NCs reported in Table S2. From Table 2, it appears that the gas phase NPs exhibit excitation energies mostly around 3.1-3.2 eV, which is only higher than the optical gap for bulk anatase (~3.0 eV); in most cases these values increase mildly in water. An exceptional behavior is noted for the rutile n = 51 NP, for which the optical gap is much lower than for the other NPs and near the visible part of the spectrum. The PBE0 excitation energies are considerably higher than the PBEx ones (see Table S3), with values in general around 3.8-4.0 eV both in gas phase and in water although for the latter they tend to be slightly higher. The case of the rutile n = 51 NP is different, for which the calculated values are around 3.0 eV. Both PBEx and PBE0 sets of values seem reasonable in view of the anatase bulk optical gap, which means that the first excited singlet does not correspond to a spurious long-range charge transfer state. However, the rutile n = 51 NP presents a different behavior, with the optical gap at the PBEx level being significantly lower than the rutile bulk limit of about

3.0 eV due to the surface effects.[72] The increase of excitation energies with the amount of Fock exchange is commonly found for TDDFT in singlet excitation calculations.

In Table S2, one can see that the values of TDDFT excitation energies for the NCs are larger than for the NPs, due to the quantum confinement effect as expected. In fact, values between 3.0 and 4.0 eV are found at the PBEx level, increasing up to 4.3 eV in water solvation but in many cases being around 4.0 eV. For the PBE0 density functional, the gas phase values for the NCs are mostly between 4.0 and 4.6 eV, with water solvation tending to homogenize the energies, which cluster around 4.5-4.7 eV. It is noticeable the larger effect of the solvent for the NCs than for the NPs, which can be explained by the former having many of their atoms on the surface.

It is interesting to analyze the character of the first excited state as expressed in the canonical Kohn-Sham MO basis as well as the differences when the excitation is expressed in terms of the NTOs. Let us focus first on the canonical MO basis. Many of TiO_2 NPs present a HOMO-LUMO single excitation as the main character of the electronic transition as compiled in Table 2, but the n = 78 NP is sometimes an exception, showing a HOMO-1-LUMO predominant character in the gas phase. Among the stoichiometric NPs, the one with n = 165 is particularly interesting since several single excitations contribute to the transition in the canonical MO basis. Also, for the gas phase reduced 84_I-3-2 NP, even though the HOMO-LUMO transition is the most important one, its contribution at the PBE0 level is as low as 25%. However, the weight of the first pair of NTOs in the first excited state is always larger than 80%, and in many cases, it is close to 100%. This fact evinces the much more compact expression of the excited state in terms of NTOs than in the canonical MO basis, which facilitates the understanding of the electronic structure changes in the transition.

The character of the electronic transition for the NCs is more varied, especially at the PBE0 level (Table S3). Indeed, at the PBEx level (Table S2), many NCs show a very predominant HOMO-LUMO single excitation, but some of them present transitions with participation of HOMO-1 and LUMO+1 canonical MOs. However, in most cases, the first pair of NTOs has an almost 100% weight but note the cases of n = 12 and 18 for gas phase, and of those two plus n = 20 for water solvation. Here, the electronic transition is split between two dominant NTO pairs, which means that even in the NTO basis the transition cannot be further simplified. It is noteworthy that PBE0 yields a very different character for the transition in canonical MOs as compared to PBEx, with many MOs between HOMO-5 and LUMO+4 contributing and a quite disperse character in general. For most NCs there is a single pair of dominant NTOs for PBE0, but for the n = 4, 8, 12, 18, 19, and 20 NCs there are two dominant pairs of NTOs.

The charge separation in the excited state can be made evident by plotting NTOs and centroids in real space. In what follows we analyze the different behavior of particular NCs and NPs focusing especially on the effect of solvation. In Fig. 4, NTOs and centroids are represented for n = 5, 11, 16, and 20 at the PBEx level. The PBEx and PBE0 NTOs for all NCs are presented in Fig. S1 and S2, respectively and the PBEx centroids are presented in Fig. S4. For the n = 5 NC, the hole NTO is different in the gas phase and in water, whereas

the electron NTO is almost identical in both cases. Note the corresponding change in the hole centroid. This can be considered a case with a local excitation character, in agreement with the values of the descriptors in Table 1. The n = 11 NC differs in both NTOs when one changes from gas phase to water, and both of them shift from one side of the cluster to the other one for what is a moderately long-range charge transfer. Note that it would not be possible to differentiate the transition by invoking the descriptors only, as they are quite similar in gas phase and in water. The n = 16 NC is a case where a long-range charge transfer in gas phase turns into a local excitation in water. For the former, the centroids are on opposite sides of the cluster, and for the latter they almost coincide. This is reflected on the value of Φ_S, changing from 0.13 in gas phase to 0.32 in water (see Table 1). Finally, for the n = 20 NC the first excitation corresponds to a local transition with a large electron/hole overlap and very close centroids in gas phase and water, with almost identical NTOs. This is the largest NC and the influence of the surface atoms is quite small.

Next, we focus on Fig. 5 to analyze the PBEx derived NTOs and centroids for the n = 78, 84, 97, and 84_I-3-2 NPs. The PBEx and PBE0 derived NTOs for all NPs are reported in Fig. S3, and the centroids in Fig. S5. The bipyramidal n = 84 NP presents hole and electron NTOs which are concentrated in layers of atoms in the equatorial region, and do not vary significantly between gas phase and water. The centroids are also close to the center of the NP. Interestingly, the character of the exciton is quite similar to that of the bulk anatase exciton, where it was found experimentally that it has a quasi-2D electron density with the electron density in a layer of atoms.[73] The n = 78 NP has a truncated octahedral shape exposing both (101) and (001) surfaces, hence it is not unexpected that the hole NTOs is quite different to the one observed for the n = 84 NP and in fact, it is located on the nanoparticle surface. The anatase bipyramidal n = 35 and 84 NPs show an interesting electronic effect. For these NPs, there are two energetically close isomers that differ essentially in having straight or tilted apical Ti-O bonds. In the present work we have studied the isomers with straight Ti-O bonds and, for both of them, the exciton is qualitatively similar to the anatase bulk one, as just explained. However, in a recent nonadiabatic molecular dynamics (NAMD) study by Prezhdo *et al.*,[15] the authors investigated the tilted apical n = 35 and 84 isomers with the PBE density functional and a plane-wave basis set. They found that the first excited state has a HOMO-LUMO character and the HOMO has its electron density centered on the apical oxygen atom, different to the quasi-2D HOMO found here. On the other hand, the LUMO for both isomers reported by Prezhdo *et al.*[15] has a quasi-2D shape as in the present work involving the NPs with straight Ti-O apical bonds. For the two other NPs in common between the present study and that of Prezhdo *et al.*,[15] namely, the cuboctahedral n = 78 and 97 NPs, results in both studies are qualitatively similar.

Since the discrepancies found for the isomers with n = 35 and 84 would lead, in principle, to quite different charge separation and recombination, we have further investigated the origin of the discrepancy. To this end, additional TDDFT calculations were carried out for the smaller, n = 35 NP in straight and tilted apical configurations, using the PBE, PBEx and PBE0 density functionals with the 6-31G* basis set. For the PBE density functional, as also employed by Prezhdo *et al.*[15], we found that the MO centered on the apical oxygen

corresponds to LUMO+7 and to HOMO-2 canonical MOs in the straight and the tilted apical configuration, respectively. For the PBEx and PBE0 density functionals, the apical oxygen MO corresponds to LUMO+9 and LUMO+11 for the straight bond isomer, respectively, and to HOMO-2 for the tilted apical MO for both density functionals. Thus, even for the tilted apical configuration, it seems that the electronic structure is quite sensitive to the method, in particular to the basis set, and that the character of the first excited state depends on the detailed parameters employed.

The cases of the anatase cuboctahedral $n = 97$ and the rutile $n = 51$ NPs deserve separate analysis. For the $n = 97$ NP, the (101) and (001) facets have a more similar surface area than for the other NPs, and for the $n = 51$ NP, the three different (101), (110), and (100) surfaces are present. For $n = 97$, in the gas phase the hole NTO is located on the top (001) NP surface, whereas the electron NTO has its maximum density towards the inner atoms. The situation changes in water, with the hole NTO acquiring an inner particle character and the electron transition being now more similar to the ones for the $n = 78$ and 84 NPs. For n = 51, both in the gas phase and in water, the NTOs are also quite different, with the hole NTO located on the surface and the electron NTO inside the NP. Finally, for the 84_I-3-2 reduced NP, the hole NTO is strongly located around the oxygen vacancy atom, with the electron NTO again peaking around the central atoms of the NP. Thus, we can conclude that the $n = 97$ NP in the gas phase, and especially the $n = 51$ NP both in the gas phase and in water (because of its low optical gap, see above), seem to be the most interesting from the point of view of charge separation and could be good candidate NPs for further study related to photocatalysis. In contrast, the first excitation in bipyramidal NPs appears to be essentially anatase bulk-like.

The above discussion can be related to some recent experiments on photocatalysis in truncated NPs,[74-76] whereby it has been shown that coexposed (001) and (101) facets of anatase NPs lead to enhanced photocatalytic activity. This finding has also been the subject of recent theoretical work on the interface between those facets.[77,78] It has also been shown that upon photoexcitation, holes tend to concentrate on the top (001) facet, whereas electrons migrate to the (101) facet. This gives rise to oxidation on the (001) facet with concomitant reduction on the (101) facet, but the largest activity is observed in edges and corners of the NP.[76] Altogether, these studies suggest that NPs such as the anatase $n = 97$ and rutile $n = 51$ NPs presented here should give rise to especially strong photocatalysis. Although these NPs are still small from an experimental point of view, their first singlet excited state character seems appropriate to yield the same effect observed experimentally. In our view, this tends to corroborate the present theoretical study as to the methodology employed.

As mentioned above, in some cases the expansion of the excited state wave function in a canonical Kohn-Sham MO basis is quite different to the expansion in an NTO basis. Therefore, the MOs participating in the transition are also expected to be different from the NTOs. For the $n = 16$ NC in water (Fig. 6), we compare the HOMO and LUMO MOs, which participate in the main single excitation for the excited state, with the first pair of NTOs. The corresponding MO and NTO coefficients in the present basis set expansion are reported in Table S2. Here, the HOMO is essentially identical to NTO1, but the LUMO is quite different

to NTO2. This can be understood from the coefficients listed in Table S2, as the contribution of the HOMO-LUMO single excitation to the excited state has a weight of 48% only whereas the second transition involves HOMO again but also LUMO+1. The n = 97 NP in water can also be analyzed in a similar way and the HOMO, LUMO, NTO1 and NTO2 are shown in Fig. 6. In this case, the LUMO and NTO2 are similar but the HOMO and NTO1 are different, with NTO1 having an electron density located towards the geometric center of the NP and HOMO having a density located more towards the edges. In this case, LUMO participates in both main excitations, but HOMO only participates in one of them, with HOMO-3 being excited in the other one.

The discussion above shows that the calculation of NTOs leads sometimes to a drastic simplification of the electronic transition character, which facilitates the analysis concerning the regions of a particular molecule or cluster involved in charge transfer. This effect is quite remarkable in the case of PBE0 calculations for the NCs, which have a very disperse nature when they are expressed in the canonical MO basis but in general, a simple expression in terms of a single pair of NTOs. Thus, in many cases NTOs offer an electron/hole picture of the excitations which, along with the topological descriptors, should facilitate a first assessment of the potential of a NP for long-range charge separation and photocatalysis.

3.3. Long-range corrected CAM-B3LYP *versus* global hybrids

To further assess the effect of introducing a long-range correction in the density functional, we have performed additional TDDFT calculations with the CAM-B3LYP functional which was designed to properly handle charge-transfer excitations. In particular, we have chosen the $(TiO_2)_n$ NPs with n = 35 and 97 because, according to the TDDFT PBEx and PBE0 calculations presented above and to the NTOs shown in Fig. S3, they represent one case with a small charge separation (n = 35) and one with a large charge separation (n = 97). First, the optical gap obtained with TDDFT CAM-B3LYP for these NPs is 4.10 and 4.37 eV for the n = 35 NP, for gas phase and water, respectively, and 4.40 and 4.41 eV for the n = 97 NP, again for gas phase and water. One can compare these values with those obtained with PBEx (Table 2), namely, 3.12 and 3.19 eV for the n = 35 NP, and 3.08 and 3.29 eV for the n = 97 NP, and with those obtained with PBE0 (Table S3): 3.77 and 3.85 eV for the n = 35 NP, and 3.91 and 3.96 eV for the n = 97 NP. Overall, this seems to reflect the tendency of TDDFT calculations to yield larger optical gaps when the percent of Fock exchange increases, as noted above and since CAM-B3LYP has a 65% of Fock exchange in the long range. On the other hand, the NTOs obtained at the CAM-B3LYP level are presented in Fig. 7. Comparing with the NTOs in Fig. S3, one can observe that the former is qualitatively different to the ones obtained with the global hybrids in the gas phase, whereas they are similar if the calculations are carried out in water solvent. In our view, this does not necessarily mean that the first singlet excited state obtained by global hybrids is spurious, as the precise character of that electronic state could depend sensitively on the density functional. Furthermore, the above discussion on the anatase n = 97 and rutile n = 51 NPs suggests that the character of the first singlet excited state as found in TDDFT global hybrid calculations is qualitatively correct. In the absence of a thorough study of this issue, we remark that the main aim of the present work is to explore the information provided by

topological descriptor-based approach so as to assess the character of the electronically excited states of TiO_2 NPs. The final goal being orient the search of the most (and least) promising NPs in photocatalysis. We hope that our work can inspire further theoretical research into this very important topic.

4. Conclusions

In the present work we have characterized the first excited state of a series of TiO_2 NCs and NPs with the help of three topological descriptors (indicating charge transfer degree, charge density overlap, and distance between centroids of charge) and with an expansion of the electronic transition in terms of natural transition orbitals (NTOs).

For the $(TiO_2)_n$, n = 1-20 NCs, topological descriptors reveal an important reduction in charge transfer character of the exciton with water solvation, at least for the continuum solvation model employed here. A feature also encountered in the larger NPs although in a lesser extent. In most cases, a single pair of NTOs is able to describe the electronic transition, which in some cases, especially for the PBE0 density functional, affords a drastic simplification and a better view of the displacement of charge density.

For the NPs, different types of excitation have been found. For the anatase bipyramidal n = 35, 84, and 165 NPs, the exciton is located as quasi-2D layers close to the equator of the bipyramid. Thus, a rather local excitation far from the surface of the NPs can be predicted. The fact that, for a different isomer than the one studied here for the n = 35 and 84 NPs, previous work based on NAMD found a rather large charge separation may indicate that a tiny structural difference may have a very large impact in the nature of the first excited state. Additional TDDFT calculations performed here for n = 35 reveal that the exciton character is very sensitive to the density functional and basis sets employed. Therefore, charge separation and recombination in these particular NPs possibly warrants further study. The cases of the anatase cuboctadedral n = 97 and the rutile n = 51 NPs are particularly interesting since the hole is clearly located on the surface of the NPs and the electron is located inside the NPs which may have strong implications to their photocatalytic activity. Recent experimental work on truncated NPs agree with this finding. From additional calculations for the n = 35 and n = 97 nanoparticles we have shown that CAM-B3LYP provides qualitatively different NTOs compared to the global hybrids. Clearly, the dependence of the character of electronic excited states of TiO_2 nanoparticles on the density functional, as described by TDDFT, and, in particular, on the percent of Fock exchange, warrants further study.

The present work provides evidence that the analysis of topological descriptors and NTOs offer important information on the nature of the excited states. This information together to the calculated excitation energies may provide indications to the experimentalists aimed at the rational synthesis of photocatalytic TiO_2 NPs. Here, it is important to recognize that the tools in the present work allow one to discriminate NPs in terms of excitation energy and character of the excited state. However, a large hole-electron separation is a necessary but not sufficient condition for efficient photocatalysis. In this sense, the NAMD studies reported by Prezhdo et *al*.[15] constitute one more step to assess the potential of TiO_2 NPs is in photocatalysis.

Finally, note that even if the present study focused on TiO_2 NPs, the reported computational strategy and analysis tools can be applied to other semiconducting oxide nanoparticles with potential photocatalytic activity although it is advised to control the quality of the basis set chosen and make sure that the density functional selected provides a qualitatively correct description of the electronic structure of the systems to be investigated.

Conflicts of interest

There are no conflicts of interest to declare.

Acknowledgements

The authors are indebted to Prof. Thibaud Etienne for valuable discussions on the usage of NANCY_EX-2.0 software. This research was supported by the Spanish MICIUN RTI2018-095460-B-I00 grant and, in part, by Generalitat de Catalunya (grants 2014SGR97 and XRQTC) and by Spanish Structures of Excellence *María de Maeztu* program through grant MDM-2017-0767. A. M. G. thanks to Spanish MICIUN for the *Juan de la Cierva* postdoctoral grant (IJCI-2017-31979) and F. I. acknowledges additional support from the 2015 ICREA Academia Award for Excellence in University Research. Computational time at the MareNostrum supercomputer has been provided by the Barcelona Supercomputing Centre through grants from *Red Española de Supercomputación* and the EXCIPHOCAT project 2016163940 of the Partnership for Advanced Computing in Europe (PRACE).

Table 1. Topological descriptors for $(TiO_2)_n$, n = 1-20 NCs and n = 35, 78, 84, 84_I-3-2, 97, and 165 (anatase), and n = 51 (rutile) NPs as obtained from hybrid TDDFT PBEx density functional calculations.

$(TiO_2)_n$ units	Φ		Φ_S		d_c / Å	
	Gas phase	Water	Gas phase	Water	Gas phase	Water
1	0.92	0.89	0.25	0.30	1.67	0.87
2	0.88	0.88	0.33	0.32	0.00	0.00
3	0.98	0.92	0.12	0.29	3.58	1.56
4	0.92	0.90	0.27	0.30	1.19	0.63
5	0.89	0.83	0.31	0.43	1.29	0.80
6	0.89	0.86	0.29	0.36	2.43	1.23
7	0.92	0.84	0.23	0.38	3.18	0.39
8	0.91	0.84	0.29	0.40	0.00	0.00
9	0.92	0.87	0.25	0.35	3.74	1.10
10	0.86	0.86	0.37	0.37	0.06	0.33
11	0.90	0.89	0.29	0.29	3.76	3.01
12	0.94	0.87	0.22	0.36	3.29	0.08
13	0.93	0.90	0.23	0.29	4.32	0.46
14	0.94	0.91	0.19	0.28	3.97	1.03
15	0.95	0.95	0.18	0.18	4.71	4.49
16	0.97	0.89	0.13	0.32	9.09	0.68
17	0.96	0.91	0.16	0.26	4.89	2.02
18	0.93	0.89	0.23	0.29	2.77	0.05
19	0.88	0.88	0.32	0.34	1.83	0.76
20	0.86	0.86	0.39	0.40	0.06	0.30
35	0.92	0.92	0.28	0.29	0.85	0.86
78	0.88	0.88	0.38	0.38	0.59	0.57
84	0.91	0.91	0.33	0.33	1.11	1.10
97	0.96	0.89	0.21	0.36	4.61	0.75
165	0.89	0.89	0.37	0.38	0.51	0.71
84 I-3-2	0.89	0.89	0.34	0.32	2.61	2.74
51	0.96	0.95	0.14	0.16	0.03	0.07

Table 2. TDDFT PBEx/6-31G(d) optical gaps, excited state character, and weight of NTOs for the $(TiO_2)_n$, n = 35, 78, 84, 97, 165, and 84_I-3-2 (anatase) and n = 51 (rutile) NPs.

	Optical gap / eV	Excited state character	Weight of NTOs 1 and 2
		Gas phase	
35	3.12	HOMO – LUMO 93%	97%
78	3.19	HOMO-1 – LUMO 79%	97%
84	3.14	HOMO – LUMO 92%	97%
97	3.08	HOMO – LUMO 95%	98%
165	3.18	HOMO – LUMO 18% HOMO-2 – LUMO 30% HOMO-4 – LUMO 37%	95%
84-I-3-2	0.64	HOMO – LUMO 80%	100%
51	2.29	HOMO – LUMO 87%	95%
		Water	
35	3.19	HOMO – LUMO 93%	97%
78	3.21	HOMO – LUMO 91%	97%
84	3.17	HOMO – LUMO 92%	97%
97	3.29	HOMO – LUMO 50% HOMO-3 – LUMO 30%	95%
165	3.16	HOMO – LUMO 23% HOMO-2 – LUMO 27% HOMO-4 – LUMO 27%	95%
84-I-3-2	0.31	HOMO – LUMO 77%	100%
51	2.43	HOMO – LUMO 74%	96%

Fig. 1. Difference between Φ values for gas phase and water solvated NCs, $(TiO_2)_n$, n = 1-20 for TDDFT PBEx calculations.

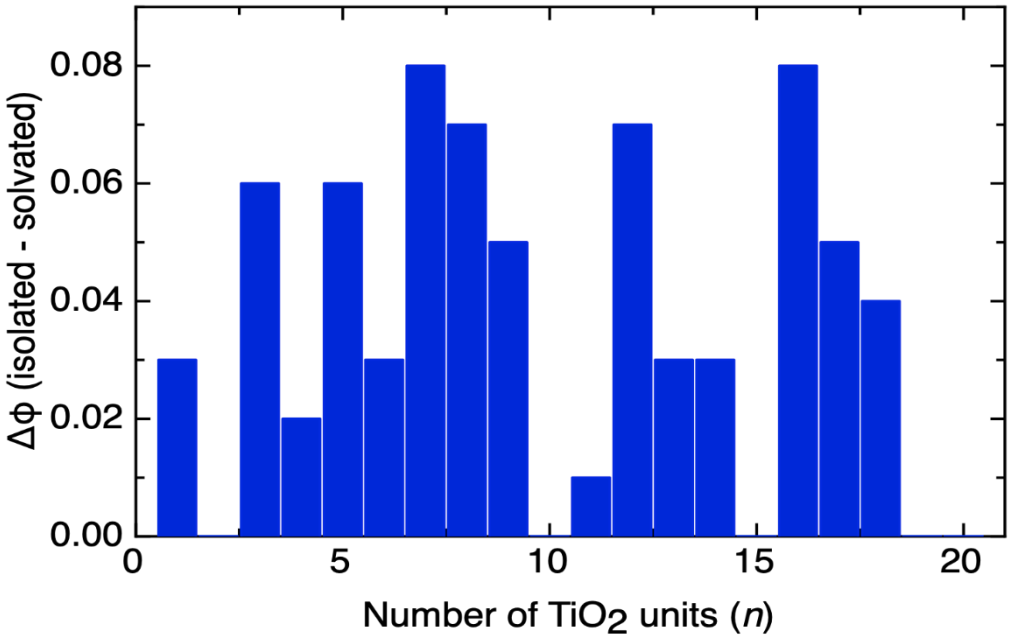

Fig. 2. Difference between Φ_S values for gas phase and water solvated NCs, $(TiO_2)_n$, n = 1-20 for TDDFT PBEx calculations.

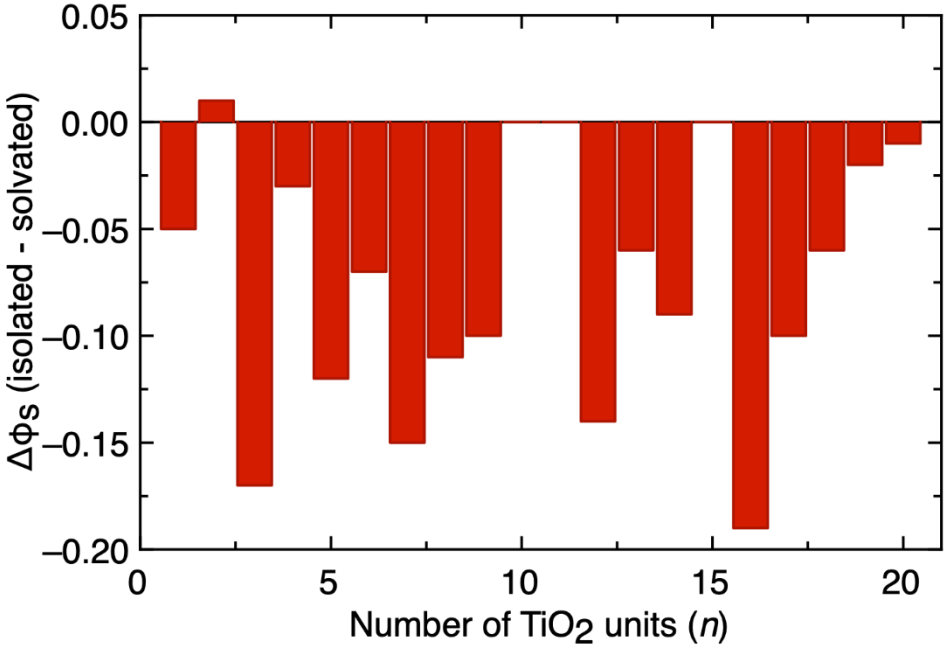

Fig. 3. Centroid distance *versus* Φ_S and Φ for gas phase and water solvated NCs, $(TiO_2)_n$, n = 1-20 for the TDDFT PBEx calculations.

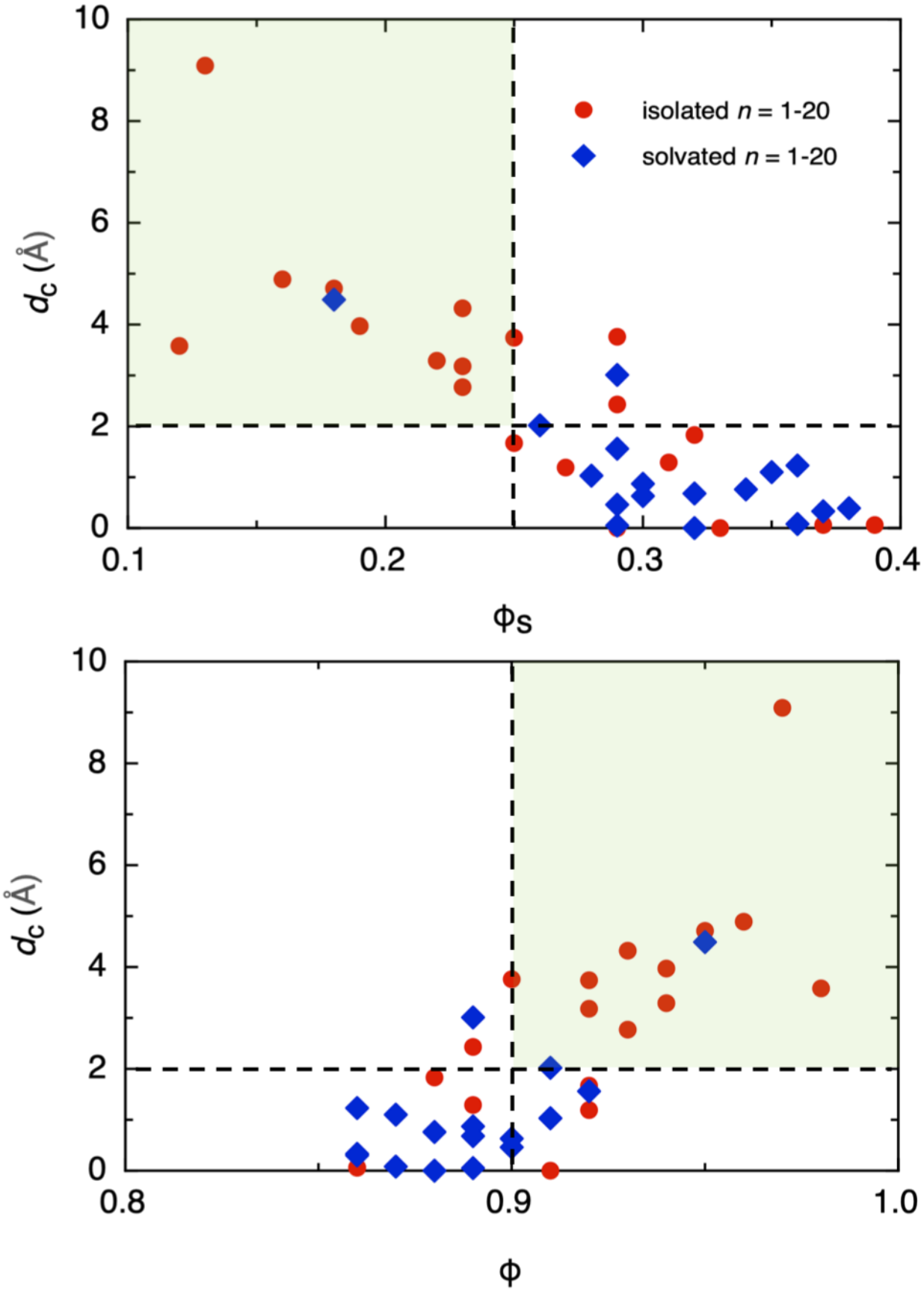

Fig. 4. NTOs and centroids for n = 5, 11, 16, and 20 corresponding to the hybrid TDDFT PBEx density functional, in gas phase and water. Left upper panel: n = 5; right upper panel: n = 11; left lower panel: n = 16; right lower panel: n = 20. For all panels, gas-phase NTOs and centroids are presented above and solvent ones below. The blue and pink spheres represent the positive (hole) and negative (electron) centroids, respectively. For NTOs, the grey and red spheres represent titanium and oxygen atoms, respectively, and for centroids, they are represented as green and red sticks, respectively.

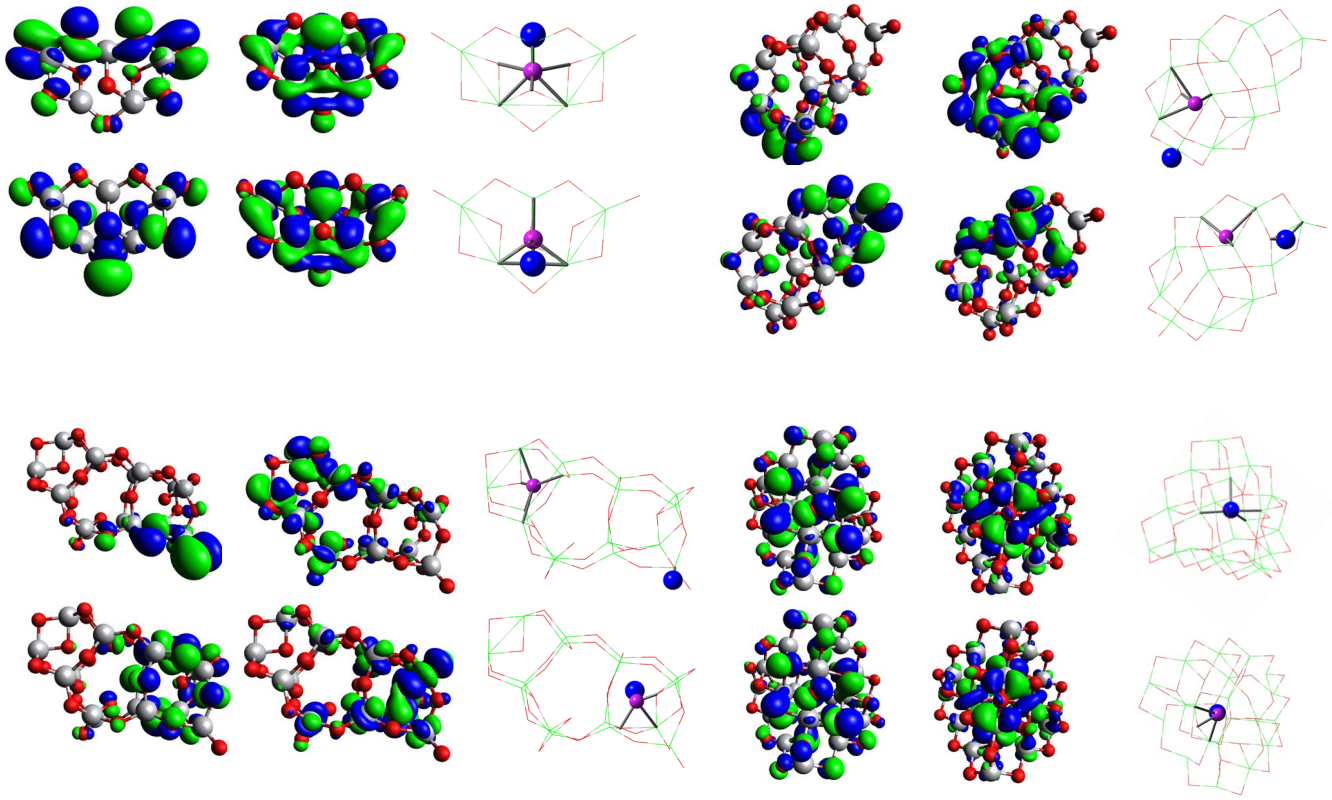

Fig. 5. NTOs and centroids for n = 84, 78, 97, and 84_I-3-2 (anatase) and n = 51 (rutile) in the gas phase and water, as predicted from the hybrid TDDFT PBEx calculations. Left upper panel: n = 84; right upper panel: n = 78; left central panel: n = 97; right central panel: n = 84_I-3-2; lower panel: n = 51. The blue and pink spheres represent the positive (hole) and negative (electron) centroids, respectively. For all panels, gas-phase NTOs and centroids are presented above and solvent ones below. For NTOs, the grey and red spheres represent titanium and oxygen atoms, respectively, and for centroids, they are represented as green and red sticks, respectively.

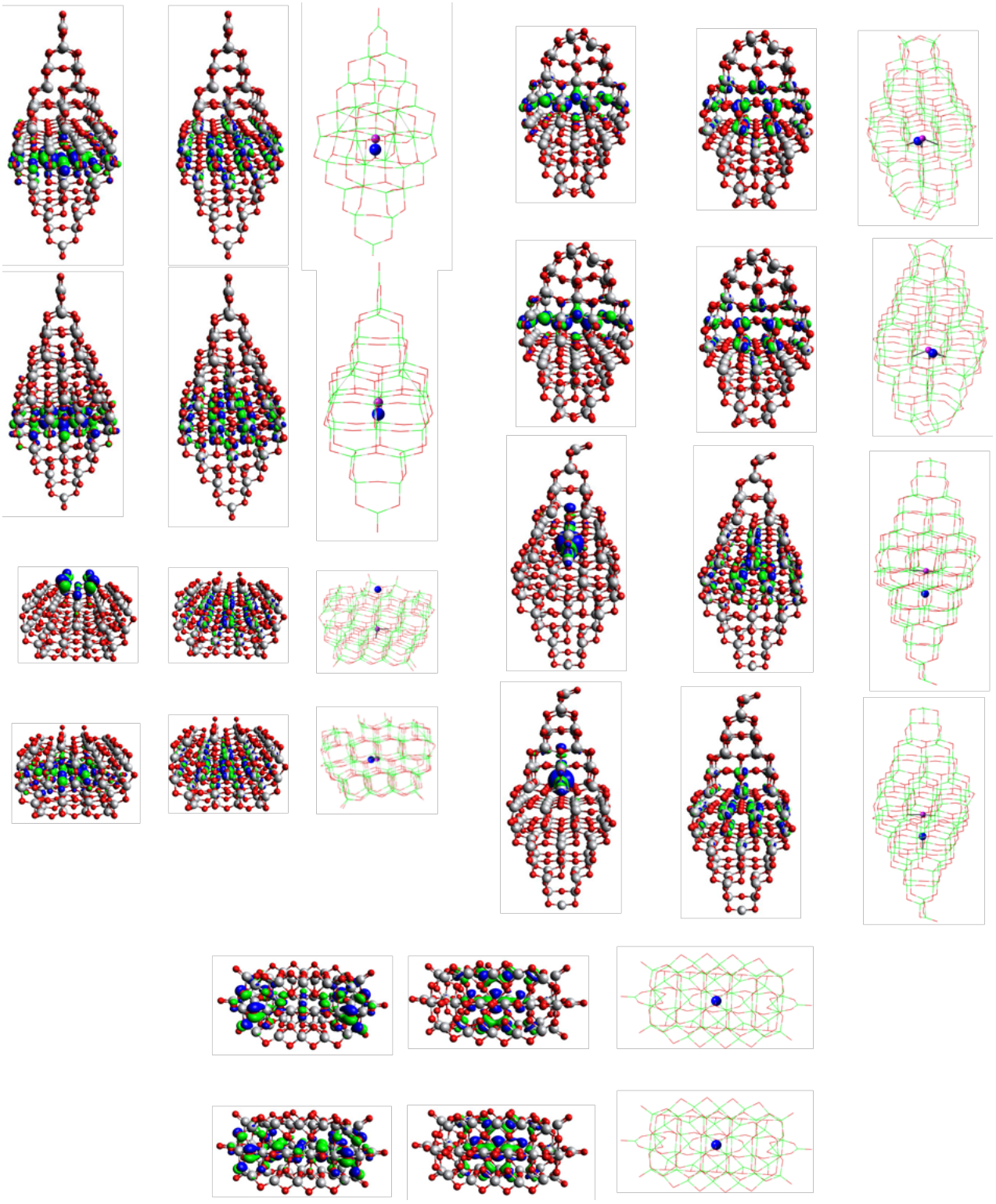

Fig. 6. HOMO and LUMO Kohn-Sham MOs and first pair of NTOs for the n = 16 NC in water, and for the n = 97 NP in water as predicted from the hybrid TDDFT PBEx calculations. Upper panel: n = 16; lower panel: n = 97. The grey and red spheres represent titanium and oxygen atoms, respectively.

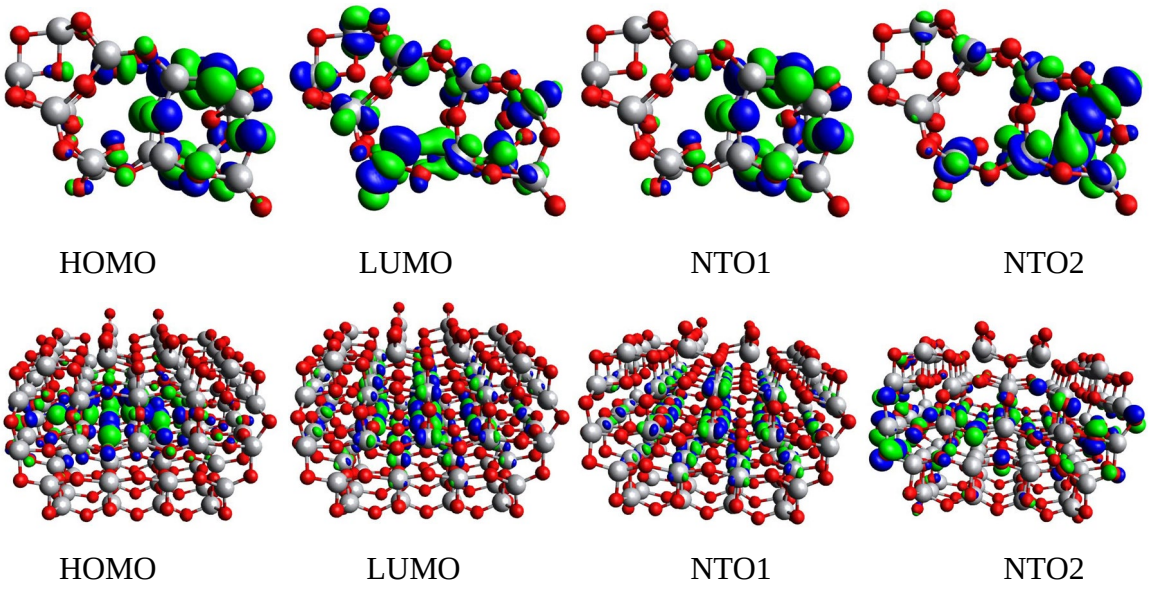

Fig. 7. First pair of NTOs for the *n* = 35 and n = 97 NPs in gas phase and in water as predicted from the long-range corrected TDDFT CAM-B3LYP calculations. Upper panel: *n* = 35; lower panel: *n* = 97. In both cases, gas phases NTOs are on the left and solvent NTOs are on the right. The grey and red spheres represent titanium and oxygen atoms, respectively.

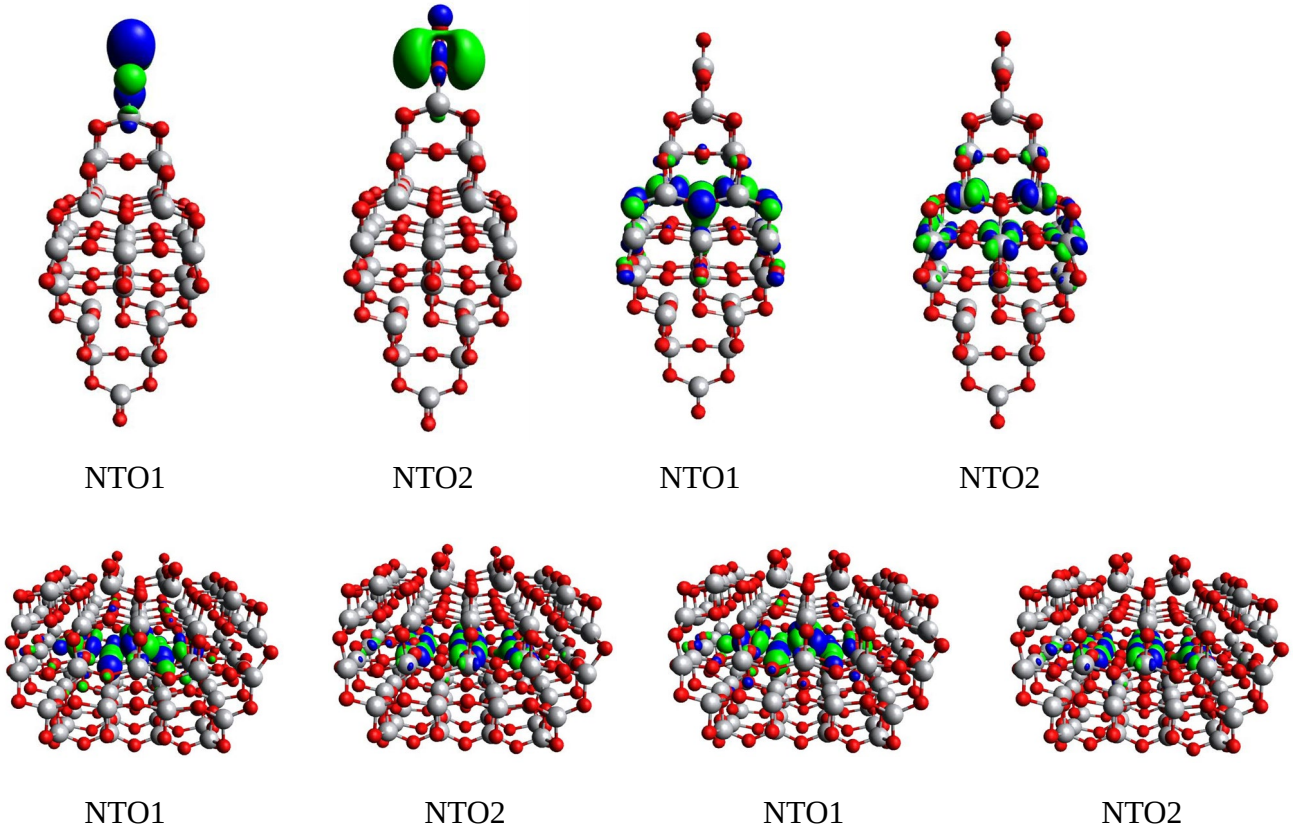

REFERENCES

1 A. Fujishima and K. Honda, Electrochemical Photolysis of Water at a Semiconductor Electrode, *Nature*, 1972, **238**, 37-38.

2 A. Fujishima, T. N. Rao and D. A. Tryk, Titanium Dioxide Photocatalysis, *J. Photochem. Photobiol. C,* 2000, **1**, 1-21.

3 A. Fujishima, X. Zhang and D. A. Tryk, TiO_2 Photocatalysis and Related Surface Phenomena, *Surf. Sci. Rep.*, 2008, **63**, 515-582.

4 M. Ni, M. Leung, D. Leung and K. A. Sumathy, Review and Recent Developments in Photocatalytic Water-Splitting Using TiO_2 for Hydrogen Production, *Renewable Sustainable Energy Rev.*, 2007, **11**, 401-425.

5 J. Schneider, M. Matsuoka, M. Takeuchi, J. Zhang, Y. Horiuchi, M. Anpo and D. W. Bahnemann, Understanding TiO_2 Photocatalysis: Mechanisms and Materials, *Chem. Rev.*, 2014, **114**, 9919-9986.

6 A. Kudo and Y. Miseki, Heterogeneous Photocatalyst Materials for Water Splitting, *Chem. Soc. Rev.*, 2009, **38**, 253-278.

7 M. A. Henderson, A Surface Science Perspective on TiO_2 Photocatalysis, *Surf. Sci. Rep.*, 2011, **66**, 185-297.

8 Y. Yamada and Y. Kanemitsu, Determination of Electron and Hole Lifetimes of Rutile and Anatase TiO_2 Single Crystals, *Appl. Phys. Lett.*, 2012, **101**, 133907 (1-4).

9 A. Y. Ahmed, T. A. Kandiel, T. Oekermann, K. Gunnemann and D. Bahnemann, Mechanistic Investigations of Photoelectrochemical Water and Methanol Oxidation on Well-Defined TiO_2 Anatase (101) and Rutile (110) Surfaces. *ACS Appl. Energy Mater.*, 2019, **2**, 5308-5318.

10 K. Ozawa, M. Emori, S. Yamamoto, R. Yukawa, S. Yamamoto, R. Hobara, K. Fujikawa, H. Sakama and I. Matsuda, Electron-Hole Recombination Time at TiO_2 Single-Crystal Surfaces: Influence of Surface Band Bending, *J. Phys. Chem. Lett.*, 2014, **5**, 1953-1957.

11 G. Cernutto, N. Masciocchi, A. Cervellino, G. M. Colonna and A. Guagliardi, Size and Shape Dependence of the Photocatalytic Activity of TiO_2 Nanoscrystals: A Total Scattering Debye Function Study, *J. Am. Chem. Soc.*, 2011, **133**, 3114-3119.

12 F. Amano, T. Yasumoto, O.-O. Prieto-Mahaney, S. Uchida, T. Shibayama and B. Ohtani, Photocatalytic Activity of Octahedral Single-Crystalline Mesoparticles of Anatase Titanium (IV) Oxide, *Chem. Commun.*, 2009, **0**, 2311-2313.

13 T. Bak, M. K. Nowotny, L. R. Sheppard and J. Nowotny, Mobility of Electronic Charge Carriers in Titanium Dioxide, *J. Phys. Chem. C*, 2008, **112**, 12981-12987.

14 G. Fazio, L. Ferrighi and C. Di Valentin, Photoexcited Carriers Recombination and Trapping in Spherical vs Faceted TiO_2 Nanoparticles, *Nano Energy*, 2016, **27**, 673-689.

15 Y. Nam, L. Li, J. Y. Lee and O. V. Prezhdo, Size and Shape Effects on Charge Recombination Dynamics of TiO_2 Nanoclusters, *J. Phys. Chem. C*, 2018, **122**, 5201-5208.

16 Y. Nam, L. Li, J. Y. Lee and O. V. Prezhdo, Strong Influence of Oxygen Vacancy Location on Charge Carrier Losses in Reduced TiO_2 Nanoparticles, *J. Phys. Chem. Lett.*, 2019, **10**, 2676-2683.

17 D. Cho, K. C. Ko, O. Lamiel-García, S. T. Bromley, J. Y. Lee and F. Illas Effect of Size and Structure on the Ground-State and Excited-State Electronic Structure of TiO_2 Nanoparticles, *J. Chem. Theory Comput.*, 2016, **12**, 3751-3763.

18 O. Lamiel-García, K. C. Ko, J. Y. Lee, S. T. Bromley and F. Illas, When Anatase Nanoparticles Become Bulklike: Properties of Realistic TiO_2 Nanoparticles in the 1-6 nm Size Range from All Electron Relativistic Density Functional Theory Based Calculations, *J. Chem. Theory Comput.*, 2017, **13**, 1785-1793.

19 A. Morales-García, A. Macià Escatllar, F. Illas and S. T. Bromley, Understanding the Interplay Between Size, Morphology and Energy Gap in Photoactive TiO_2 Nanoparticles, *Nanoscale*, 2019, **11**, 9032-9041.

20 O. Gritsenko and E. Baerends, Asymptotic Correction of the Exchange-Correlation Kernal of Time-Dependent Density Functional Theory for Long-Range Charge Transfer Excitations, *J. Chem. Phys.*, 2004, **121**, 655-660.

21 M. J. G. Peach, P. Benfield, T. Helgaker and D. J. Tozer, Excitation Energies in Density Functional Theory: An Evaluation and a Diagnostic Test, *J. Chem. Phys.*, 2008, **128**, 044118.

22 M. J. G. Peach and D. J. Tozer, Illustration of a TDDFT Spatial Overlap Diagnostic by Basis Function Exponent Scaling, *J. Mol. Struct.: THEOCHEM*, 2009, **914**, 110-114.

23 T. Le Bahers, C. Adamo and I. Ciofini, A Qualitative Index of Spatial Extent in Charge-Transfer Excitations, *J. Chem. Theory Comput.*, 2011, **7**, 2498-2506.

24 C. A. Guido, P. Cortona, B. Mennucci and C. Adamo, On the Metric of Charge Transfer Molecular Excitations: A Simple Chemical Descriptor, *J. Chem. Theory Comput.*, 2013, **9**, 3118-3126.

25 M. Savarese, C. A. Guido, E. Brémond, I. Ciofini and C. Adamo, Metrics for Molecular Electronic Excitations: A Comparison Between Orbital- and Density-Based Descriptors, *J. Phys. Chem. A*, 2017, **121**, 7543-7549.

26 M. Campetella, F. Maschietto, M. J. Frisch, G. Scalmani, I. Ciofini and C. Adamo, Charge Transfer Excitations in TDDFT: A Ghost-Hunter Index, *J. Comput. Chem.*, 2017, **38**, 2151-2156.

27 M. Campetella, A. Perfetto and I. Ciofini, Quantifying Partial Hole-Particle Distance at the Excited State: A Revised Version of the D_{CT} Index, *Chem. Phys. Lett.*, 2019, **714**, 81-86.

28 T. Etienne, X. Assfeld and A. Monari, Toward a Quantitative Assessment of Electronic Transitions´ Charge Transfer Character. *J. Chem. Theory Comput.* **2014**, *10*, 3896-3905.

29 T. Etienne, X. Assfeld and A. Monari, New Insight into the Topology of Excited States Through Detachment/Attachment Density Matrices-Based Centroids of Charge, *J. Chem. Theory Comput.*, 2014, **10**, 3906-3914.

30 T. Etienne, Theoretical Insights into the Topology of Molecular Excitons from Single Reference Excited States Calculation Methods, in *Excitons*, http://dx.doi.org/10.5772/66232, S. L. Pyshkin, Ed., Intech Croatia, 2018, pp 31-54.

31 T. Etienne, Probing the Locality of Excited States with Linear Algebra, *J. Chem. Theory Comput.*, 2015, **11**, 1692-1699.

32 A. Dreuw and M. Head-Gordon, Single-Reference *ab initio* Methods for the Calculation of Excited States of Large Molecules, *Chem. Rev.*, 2005, **105**, 4009-4037.

33 A. V. Luzanov, A. A. Sukhorukov and V. É. Umanskii, Application of Transition Density Matrix for Analysis of Excited States, *Theor. Exp. Chem.*, 1976, **10**, 354-361.

34 R. L. Martin, Natural Transition Orbitals, *J. Chem. Phys.*, 2003, **118**, 4775-4777.

35 S. A. Mewes, F. Plasser, A. Krylov, and A. Dreuw, Benchmarking Excited-State Calculations Using Exciton Properties, *J. Chem. Theory Comput.*, 2018, **14**, 710-725.

36 S. A. Bäppler, F. Plasser, M. Wormit and A. Dreuw, Exciton Analysis of Many-Body Wave Functions: Bridging the Gap Between the Quasi-particle and Molecular Orbital Pictures, *Phys. Rev. A: At.; Mol., Opt. Phys.*, 2014, **90**, 05251.

37 J. Wenzel and A. Dreuw, Physical Properties, Exciton Analysis, and Visualization of Core-Excited States: An Intermediate State Representation Approach, *J. Chem. Theory Comput.*, 2016, **12**, 1314-1330.

38 L. Vannay, E. Brémond, P. de Silva and C. Corminboeuf, Visualizing and Quantifying Interactions in the Excited State, *Chem. Eur. J.*, 2016, **22**, 18442-18449.

39 Y. Li and C. A. Ullrich, The Particle-Hole Map: A Computational Tool to Visualize Electronic Excitations, *J. Chem. Theory Comput.*, 2015, **11**, 5838-5852.

40 Y. Li and C. A. Ullrich, The Particle-Hole Map: Formal Derivation and Numerical Implementation, *J. Chem. Phys.*, 2016, **145**, 164107-1/6.

41 F. Plasser, M. Wormit and A. Dreuw, New Tools for the Systematic Analysis and Visualization of Electronic Excitations. I. Formalism, *J. Chem. Phys.*, 2014, **141**, 024106/1-13.

42 F. Plasser, S. A. Bappler, M. Wormit and A. Dreuw, New Tools for the Systematic Analysis and Visualization of Electronic Excitations. II. Applications, *J. Chem. Phys.*, 2014, **141**, 024107/1-12.

43 F. Plasser, B. Thomitzni, S. A. Bäppler, J. Wenzel, D. R. Rehn, M. Wormit and A. Dreuw, Statistical Analysis of Electronic Excitation Processes: Spatial Location, Compactness, Charge Transfer, and Electron-Hole Correlation, *J. Comput. Chem.*, 2015, **36**, 1609-1620.

44 F. Plasser, S. A. Mewes, A. Dreuw and L. González, Detailed Wave Function Analysis for Multirefence Methods: Implementation in the MOLCAS Program Package and Applications to Tetracene, *J. Chem. Theory Comput.*, 2017, **13**, 5343-5353.

45 J. J. Nogueira, F. Plasser and L. González, Electronic Delocalization, Charge Transfer and Hypochromism in the UV Spectrum of Polyadenine Unravelled by Multiscale Computations and Quantitative Wave Function Analysis, *Chem. Sci.*, 2017, **8**, 5682-5691.

46 S. A. Mewes and A. Dreuw, Density-Based Descriptors and Exciton Analyses for Visualizing and Understanding the Electronic Structure of Excited States, *Phys. Chem. Chem. Phys.*, 2019, **21**, 2843-2856.

47 D. Wang, H. Wang and P. Hu, Identifying the Distinct Features of Geometric Structures for Hole Trapping to Generate Radicals on Rutile TiO_2 (110) in Photooxidation Using Density Functional Theory Calculations with Hybrid Functionals, *Phys. Chem. Chem. Phys.*, 2015, **17**, 1549-1555.

48 H. Hussain, G. Tocci, T. Woolcot, X. Torrelles, C. L. Pang, D. S. Humphrey, C. M. Yim, D. C. Grinter, G. Cabailh, O. Bikondoa, A. Lindsay, J. Zegenhagen, A. Michaelides and G. Thornton, Structure of a Model TiO_2 Photocatalytic Interface, *Nat. Mater.*, 2017, **16**, 461-466.

49 A. Migani and L. Blancafort, What Controls Photocatalytic Water Oxidation on TiO_2 (110) Under Ultra-High-Vacuum Conditions? *J. Am. Chem. Soc.*, 2017, **139**, 11845-11856.

50 F. Jin, M. Wei, T. Chen, H. Ma, G. Liu and Y. Ma, Behavior of Photogenerated Electron-Hole Pair for Water Splitting on TiO_2 (110), *J. Phys. Chem. C*, 2018, **122**, 22930-22938.

51 X. Zhou and H. Dong, A Theoretical Perspective on Charge Separation and Transfer in Metal Oxide Photocatalysts for Water Splitting, *ChemCatChem*, 2019, **11**, 1-29.

52 E. Berardo, H.-S. Hu, S. A. Shevlin, S. M. Woodley, K. Kowalski and M. A. Zwijnenburg, Modeling Excited States in TiO_2 Nanoparticles: On the Accuracy of a TD-DFT Based Description, *J. Chem. Theory Comput.*, 2014, **10**, 1189-1199.

53 E. Berardo, H.-S. Hu, H. J. J. van Dam, S. A. Shevlin, S. M. Woodley, K. Kowalski and M. A. Zwijnenburg, Describing Excited State Relaxation and Localization in TiO_2 Nanoparticles Using TD-DFT, *J. Chem. Theory Comput.*, 2014, **10**, 5538-5548.

54 R. Valero, A. Morales-García and F. Illas, Theoretical Modeling of Electronic Excitations of Gas-Phase and Solvated TiO_2 Nanoclusters and Nanoparticles of Interest in Photocatalysis, *J. Chem. Theory Comput.*, 2018, **14**, 4391-4404.

55 O. Lamiel-García, A. Cuko, M. Calatayud, F. Illas and S. T. Bromley, Predicting Size-Dependent Emergence of Crystallinity in Nanomaterials: Titania Nanoclusters *versus* Nanocrystals, *Nanoscale*, 2017, **9**, 1049-1058.

56 Á. Morales-García, O. Lamiel-García, R. Valero and F. Illas, Properties of Single Oxygen Vacancies on a Realistic $(TiO_2)_{84}$ Nanoparticle: A Challenge for Density Functionals, *J. Phys. Chem. C*, 2018, **122**, 2413-2421.

57 G. Wulff, On the Question of Speed of Growth and Dissolution of Crystal Surfaces. *Z. Krystallogr.*, 1901, **34**, 449−530.

58 K. C. Ko, O. Lamiel-García, J. Y. Lee and F. Illas, Performance of a Modified Hybrid Functional in the Simultaneous Description of Stiochiometric and Reduced TiO_2 Polymorphs, *Phys. Chem. Chem. Phys.*, 2016, **18**, 12357-12367.

59 J. P. Perdew, M. Ernzerhof and K. Burke, Rationale for Mixing Exact Exchange with Density Functional Approximations, *J. Chem. Phys.*, 1996, **105**, 9982-9985.

60 C. Adamo and V. Barone, Toward Reliable Density Functional Methods without Adjustable Parameters: The PBE0 Model, *J. Chem. Phys.*, 1999, **110**, 6158-6170.

61 J. Autschbach, Charge-Transfer Excitations and Time-Dependent Density Functional Theory: Problems and Some Proposed Solutions, *ChemPhysChem*, 2009, **10**, 1757-1760.

62 N. T. Maitra, Charge Transfer in Time-Dependent Density Functional Theory, *J. Phys.: Condens. Matter*, 2017, **29**, 432001.

63 T. Yanai, D. P. Tew and N. C. Handy, A New Hybrid Exchange-Correlation Functional using the Coulomb-Attenuating Method (CAM-B3LYP), *Chem. Phys. Lett.*, 2004, **393**, 51-57.

64 J. Tomasi, B. Mennucci and R. Cammi, Quantum Mechanical Continuum Solvation Models, *Chem. Rev.*, 2005, **105**, 2999-3093.

65 R. Cammi, B. Mennucci and J. Tomasi, Fast Evaluation of Geometries and Properties of Excited Molecules in Solution: A Tamm-Dancoff Model with Application to 4-Dimethylaminobenzonitrile, *J. Phys. Chem.* A, 2000, **104**, 5631-5637.

66 M. Cossi and V. Barone, Time-Dependent Density Functional Theory for Molecules in Liquid Solutions, *J. Chem. Phys.*, 2001, **115**, 4708-4717.

67 Gaussian 09, Revision D.01, M. J. Frisch, G. W. Trucks, H. B. Schlegel, G: E. Scuseria, M. A. Robb, J. R. Cheeseman, G. Scalmani, V. Barone, B. Mennucci, G. A. Petersson, H. Nakatsuji, M. Caricato, X. Li, H. P. Hratchian, A. F. Izmaylov, J. Bloino, G. Zheng, J. L. Sonnenberg, M. Hada, M. Ehara, K. Toyota, R. Fukuda, J. Hasegawa, M. Ishida, T. Nakajima, Y. Honda, O. Kitao, H. Nakai, T. Vreven, J. A. Montgomery, Jr., J. E. Peralta, F. Ogliaro, M. Bearpark, J. J. Heyd, E. Brothers, K. N. Kudin, V. N. Staroverov, R. Kobayashi, J. Normand, K. Raghavachari, A. Rendell, J. C. Burant, S. S. Iyengar, J. Tomasi, M. Cossi, N. Rega, J. M. Millam, M. Klene, J. E. Knox, J. B. Cross, V. Bakken, C. Adamo, J. Jaramillo, R. Gomperts, R. E. Stratmann, O. Yazyev, A. J. Austin, R. Cammi, C. Pomelli, J. W. Ochterski, R. L. Martin, K. Morokuma, V. G. Zakrzewski, G. A. Voth, P. Salvador, J. J. Dannenberg, S. Dapprich, A. D. Daniels, Ö. Farkas, J. B. Foresman, J. V. Ortiz, J. Cioslowski, D. J. Fox, Gaussian, Inc., Wallingford CT, 2009.

68 NANCY_EX. http://nancyex.sourceforge.net.

69 M. Kasha, Characterization of Electronic Transitions in Complex Molecules, *Faraday Discuss.*, 1950, **9**, 14-19.

70 M. E. Casida, Time-Dependent Density-Functional Response Theory for Molecules, in: Chong, D. P., Ed.; Recent Advances in Density Functional Methods Part I, World Scientific, Singapore, 1995, p 155.

71 I. de P. R. Moreira and F. Illas, A unified view of the theoretical description of magnetic coupling in molecular chemistry and solid-state physics, *Phys. Chem. Chem. Phys.*, 2006, **8**, 1645-1659

72 K. C. Ko, S. T. Bromley, J. Y. Lee and F. Illas, Size-Dependent Level Alignment between Rutile and Anatase TiO2 Nanoparticles: Implications for Photocatalysis, *J. Phys. Chem. Lett.*, 2017, **8**, 5593-5598.

73 E. Baldini, L. Chiodo, A. Dominguez, M. Palummo, S. Moser, M. Yazdi-Rizi, G. Aubock, B. P. P. Mallett, H. Berger, A. Magrez, C. Bernhard, M. Grioni, A. Rubio, M. Chergui, *Nat. Commun.*, 2017, **8**, 13.

74 T.-Y. Lee, C.-Y. Lee and H.-T. Chiu, Enhanced Photocatalysis from Truncated Octahedral Bipyramids of Anatase TiO_2 with Exposed {001}/{101} Facets, *ACS Omega*, 2018, **3**, 10225-10232.

75 A.-Y. Zhang, W.-Y. Zhang, J.-J. Chen, C. Liu, Q.-X. Li, X. Zhang, W.-W. Li, Y. Si and H.-Q. Yu, Epitaxial Facet Junction on TiO_2 Single Crystals for Efficient Photocatalytic Water Splitting, *Energy Environ. Sci.*, 2018, **11**, 1444-1448.

76 W.-K. Wang, J.-J. Chen, Z.-Z. Lou, S. Kim, M. Fujitsuka, H.-Q. Yu and T. Matsima, Single-Molecule and -Particle Probing Crystal Edge/Corner as Highly Efficient Photocatalytic Sites on a Single TiO_2 Particle, *Proc. Natl. Acad. Sci. U. S. A.*, 2019, **116**, 18827-18833.

77 G. Di Liberto, S. Tosoni and G. Pacchioni, Role of Heterojunction in Charge Carrier Separation in Coexposed Anatase (001)-(100) Surfaces, J. Phys. Chem. Lett., 2019, 10, 2372-2377.

78 G. Di Liberto, S. Tosoni and G. Pacchioni, Nitrogen Doping in Coexposed (001)-(101) Anatase TiO_2 Surfaces: a DFT Study, Phys. Chem. Chem. Phys., 2019, 21, 21497-21505.

TOC

Excited States Forecast

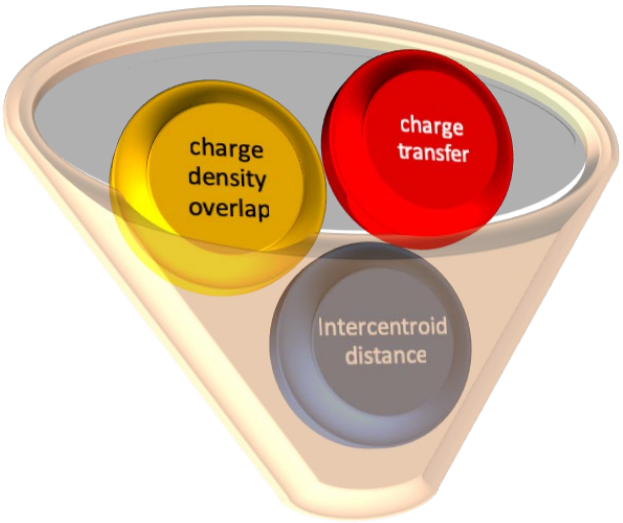

Implications for Photocatalysis